JOURNAL OF GUIDANCE, CONTROL, AND DYNAMICS
Vol. 33, No. 3, May–June 2010

Interplanetary Transfers Between Halo Orbits: Connectivity Between Escape and Capture Trajectories

Masaki Nakamiya*
Japan Aerospace Exploration Agency, Sagamihara, Kanagawa 229-8510, Japan
Hiroshi Yamakawa†
Kyoto University, Uji, Kyoto 611-0011, Japan
Daniel J. Scheeres‡
University of Colorado, Boulder, Colorado 80309
and
Makoto Yoshikawa§
Japan Aerospace Exploration Agency, Sagamihara, Kanagawa 229-8510, Japan

DOI: 10.2514/1.46446

Spacecraft escape and capture trajectories from or to Halo orbits about the $L1$ or $L2$ points using impulsive maneuvers at periapsis of the manifolds for interplanetary transfers are analyzed in the restricted Hill three-body problem. This application is motivated by future proposals to place deep-space ports at the Earth and Mars $L1$ or $L2$ points. First, the feasibility of interplanetary trajectories between Earth Halo orbits and Mars Halo orbits is investigated. In this study, unstable and stable manifolds associated with the Halo orbits are used to approach the vicinity of the planet's surface, and use impulsive maneuvers at periapsis for escape and capture trajectories to and from Halo orbits. Interplanetary trajectories between Earth and Mars Halo orbits with reasonable ΔV and flight time are found. Next, applying these dynamics to an Earth–Mars transportation system using spaceports on Earth and Mars Halo orbits, the system is evaluated in terms of the spacecraft mass of round-trip transfer. As a result, transfer between low Earth orbits and low Mars orbits via the planets' Halo orbits can reduce spacecraft wet mass compared with a direct round-trip transfer, by leaving propellant for the return.

I. Introduction

THIS paper investigates the possibility of designing realistic connections between escape trajectories from Earth Halo orbits and capture trajectories to a target planet's Halo orbit for interplanetary transfer, extending a previous paper which analyzes capture trajectories to Halo orbits of planets [1]. Moreover, an application to Earth–Mars transportation systems using spaceports at Earth and Mars Halo orbits is discussed (see Fig. 1). Assuming the construction of spaceports as candidate gateways for future interplanetary transfers at the vicinity of $L1/L2$ of the sun–Earth and sun–target body system, payloads could be transported between these spaceports by an interplanetary vehicle [1–6]. Moreover, the transportation system facilitates round-trip exploration and also leads to a reusable transportation system by supplying the interplanetary cargo ship with fuel at spaceports.

This paper is organized as follows. Sec. II briefly describes the dynamics of the Hill three-body problem. Sec. III defines escape and capture trajectories to and from Halo orbits using impulsive maneuver at periapsis of invariant manifolds and investigates the characteristics of the periapsis of manifolds. Sec. IV discusses the feasibility of linking interplanetary trajectories with stable/unstable manifolds of Halo orbits. Sec. V applies our study of escape and capture trajectories to and from Halo orbits to an Earth–Mars transportation system. The round-trip Earth–Mars transportation system using Halo orbits is then evaluated in terms of the required spacecraft wet mass.

Received 21 July 2009; revision received 14 January 2010; accepted for publication 14 January 2010.

*Postdoctoral Fellow, Department of Space Systems and Astronautics, 3-1-1 Yoshinodai; nakamiya.masaki@jaxa.jp.

†Professor, Research Institute for Sustainable Hunamosphere, Gokasho; yamakawa@rish.kyoto-u.ac.jp. Senior Member AIAA.

‡Professor, Department of Aerospace Engineering Sciences; scheeres@colorado.edu. Associate Fellow AIAA.

§Associate Professor, Department of Space Information and Energy, 3-1-1, Yoshinodai; yoshikawa.makoto@jaxa.jp.

II. Brief Description of Dynamical Model

The physical model considered in this paper is the normalized Hill model, which can be obtained from the circular restricted three-body problem by setting the center of the coordinate system to be at the secondary body and scaling the coordinates, assuming that the distance of the spacecraft from the center is small compared with the distance between the primary and secondary bodies. The resulting equations of motion provide a good description for the motion of a spacecraft in the vicinity of the $L1$ and $L2$ libration points of the secondary body [7,8]. This normalized Hill model allows us to eliminate all free parameters from the equations; thus, computations performed for them can be scaled to any physical system by multiplying by the unit length and time, which depend only on the properties of the primary and secondary bodies and their mutual orbit.

In three-dimensional space, periodic orbits called Halo orbits exist near the libration points [9–13]. The size of these periodic orbits is related to their value of the Jacobi constant, which is a conserved quantity determined from the initial conditions in the Hill model. The halo orbits of $L1$ and $L2$ are not located on the line between the primary and secondary bodies, and are not hidden in the shadow of the secondary body. Therefore, we assume that a spaceport built on a Halo orbit is able to avoid communication failures due to eclipses.

A significant additional advantage of using Halo orbits is the existence of invariant structures associated with these periodic orbits, called the unstable and stable manifolds [14,15]. These unstable and stable manifolds can be used for optimal escape and capture trajectories to and from Halo orbits as they depart from or wind onto Halo orbits with a nearly zero velocity correction [1].

In this paper our numerical computations use the Runge–Kutta–Fehlberg method with an integration error tolerance $= 1.0\text{E} - 15$. We compute Halo orbits as follows. First, we assume the initial

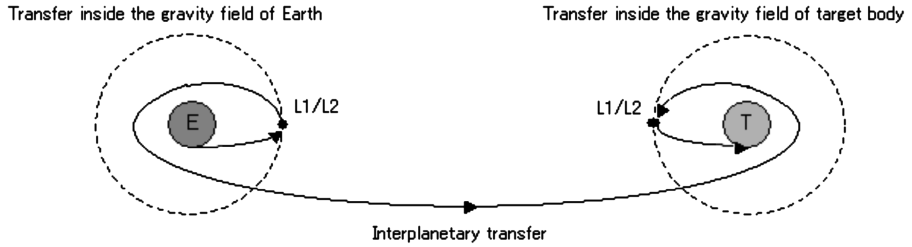

Fig. 1 Outline of an interplanetary transfer using Halo orbits [1].

conditions are $X_0 = (x_0, 0, z_0, 0, \dot{y}_0, 0)$. The equations of motion are integrated until the sign of y changes twice, and the time at this point is defined to be t. If $X_t = (x_0, 0, z_0, 0, \dot{y}_0, 0)$, that orbit is considered to be a Halo orbit (and t is considered to be the period of the Halo orbit T at this time). If the orbit does not close on itself at t, we use a minimization algorithm for nonlinear functions to drive the norm of the difference $X_t - X_0$ to zero. Moreover, invariant manifolds are generated by applying an infinitesimal impulse [0.00001 (nondim)] at different locations along the Halo orbit and integrating in time.

III. Escape and Capture Trajectories to and from Halo Orbits

A. Assumption of Escape and Capture Trajectories

In this study, we define our escape trajectories as trajectories that leave from a Halo orbit around the sun–Earth $L1/L2$ point using unstable manifolds and approach the Earth with a perigee above the Earth's surface. Subsequently, at perigee an impulsive maneuver is performed to escape from the Earth's gravitational dominance and put the spacecraft on an interplanetary trajectory. On the other hand, we define capture trajectories as trajectories that enter the sphere of influence of a target body from interplanetary space and have a close flyby with the target body. Subsequently, at periapsis of the approach hyperbola an impulsive maneuver is performed to place the spacecraft on a stable manifold that leads to capture to a Halo orbit around the sun–target body $L1/L2$, as discussed in a previous paper [1]. The reason why the impulsive maneuvers are performed at periapsis is because this location is generally the energetically efficient place to increase the escape energy or to reduce the approach energy. In this way, the unstable and stable manifolds are used for escape and capture trajectories to and from Halo orbits.

B. Characteristics of the Periapsis Points of Invariant Manifolds

Here, we investigate the periapsis passage points of unstable and stable manifolds where an impulse maneuver may be performed to transfer to and from an interplanetary transfer. The stable and unstable manifolds propagate backwards/forwards in time from the Halo orbits.

1. Periapsis Location and Minimum Periapsis Distance

In a previous paper, we investigated periapsis locations of stable manifolds for capture to the Halo orbits of a target planet [1]. We verified that the periapsis point locations of the stable manifold vary with the value of the Jacobi constant (i.e., the size of Halo orbits) and the phasing along the Halo orbit. We have obtained the relation between a minimum periapsis distance and the value of the Jacobi constant, looking across all phases of a Halo orbit. The minimum periapsis distance means the distance from the origin of the secondary body to the periapsis point of the manifold closest to the origin of the secondary, but above the surface. The minimum periapsis distance decreases as the value of the Jacobi constant increases, and the minimum periapsis distance can become smaller than the normalized mean surface radii of all the planets in the solar system for some values of the Jacobi constant for Halo orbits. The same characteristics exist for the periapsis of unstable manifolds, as the periapsis locations of stable and unstable manifolds of a Halo orbit in the Hill problem are symmetric about the x-z plane (where the x-axis is aligned with the primary and secondary bodies and centered at the secondary, the y-axis corresponds to velocity direction of the secondary and the z-axis is normal to both x and y). Thus, the stable and unstable manifold of the periapsis passage points can intersect the surface of any of the planets in the solar system (although the sizes of these Halo orbits are limited). This means that a spacecraft can depart from a Halo orbit and approach the surface of the planet with negligible velocity corrections, and wind onto a Halo orbit from a periapsis passage above the surface of the planet with negligible velocity correction (after an appropriate maneuver to transfer to the manifold).

2. Position and Velocity of Periapsis near the Surface of Planets

In this paper the position and velocity of periapsis near the surface of the Earth and Mars are investigated so that unstable manifolds of the Earth Halo orbits and stable manifolds of Mars Halo orbits can be linked. The time of flight (TOF) from a Halo orbit to periapsis can be different (e.g., a fast transfer of $P_f = 1.74$ years and a slow transfer of $P_s = 1.86$ years). We find fast transfers and slow transfers that have the same altitude of periapsis (P_f and P_s) for the same size of Halo orbits, as shown in Figs. 2 and 3. These are obtained by analyzing different initial positions along a given Halo orbit.

Figures 4 and 5 show the position and the speed at periapsis of the Earth $L1$ unstable manifolds near the Earth's surface (altitude = 300 km) as a function of the Jacobi constant in the sun–Earth fixed frame. The x and y components of the position and velocity of Earth's $L2$ unstable manifold are symmetric to the $L1$ unstable manifolds. According to Fig. 5, since the z component of velocity increases as the value of the Jacobi constant (i.e., the size of Halo orbits) increases, we are biased towards selecting small-size Halo orbits to reduce the connecting ΔV between the Earth unstable manifolds and the interplanetary trajectories. At this time, the y direction component of velocity is positive for a small value of the Jacobi constant. We wish to orient this direction so it aligns with the periapsis velocity direction that leads to the desired departure excess hyperbolic velocity vector. This also relates to the selection of either the $L1$ or $L2$ unstable manifolds to connect with the desired interplanetary trajectory. We will discuss the details in the next section.

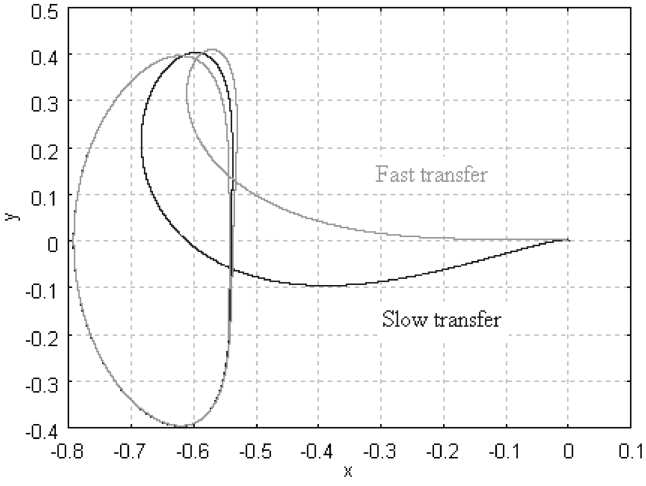

Fig. 2 Fast and slow transfers between the planet's periapsis and the Halo orbit.

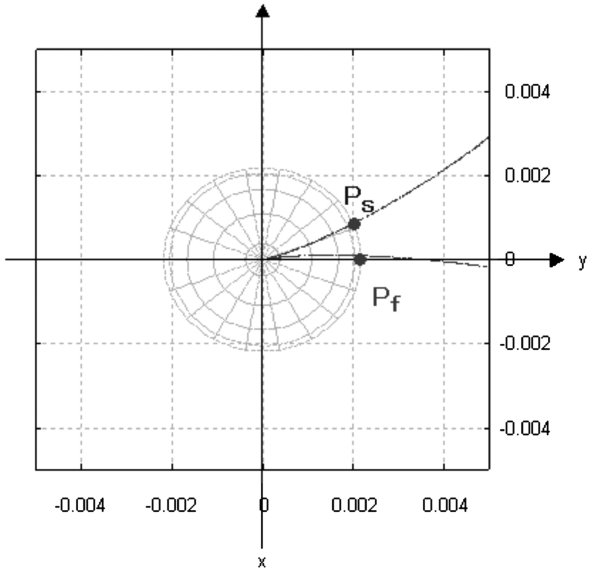

Fig. 3 Periapsis of fast and slow manifold transfers.

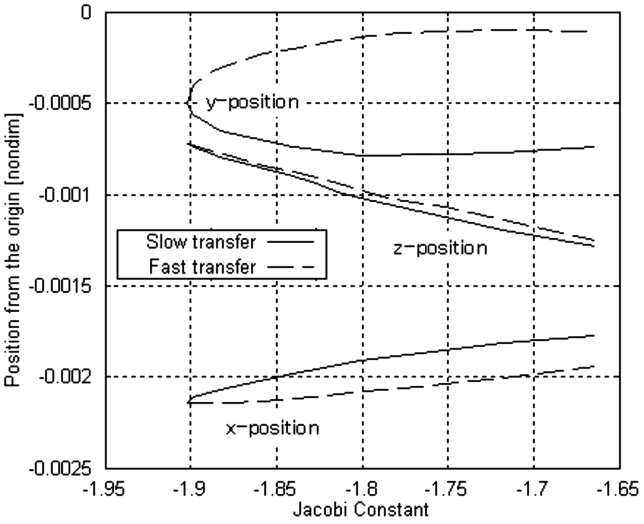

Fig. 6 Position of periapsis of Mars *L*2 stable manifold as a function of the Jacobi constant.

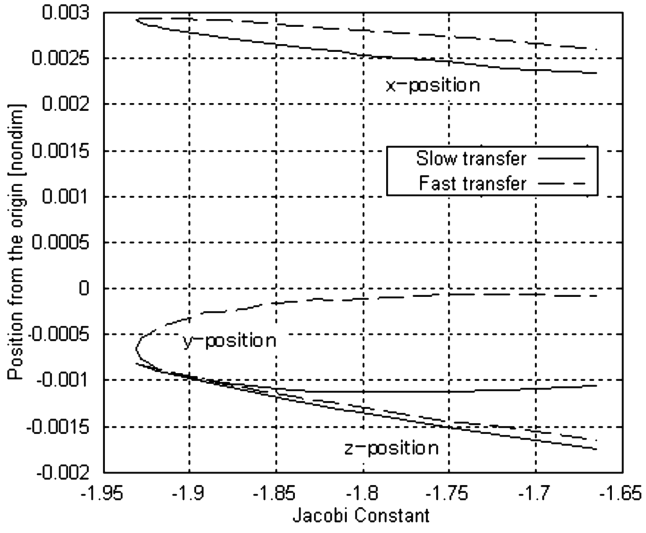

Fig. 4 Position of periapsis of Earth *L*1 unstable manifolds as a function of the Jacobi constant.

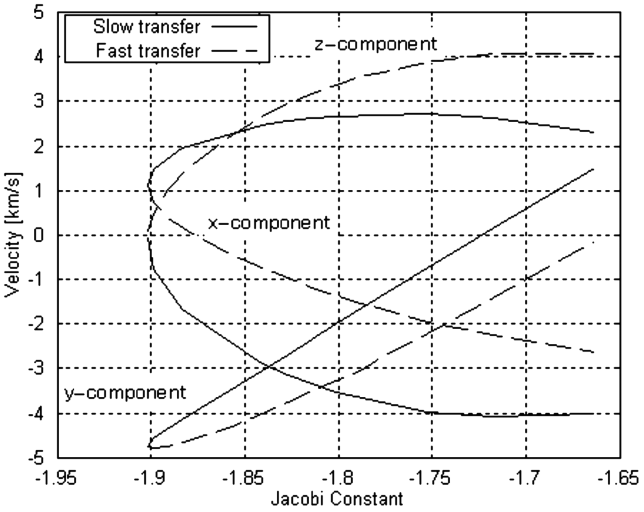

Fig. 7 Velocity of periapsis of Mars *L*2 stable manifold as a function of the Jacobi constant.

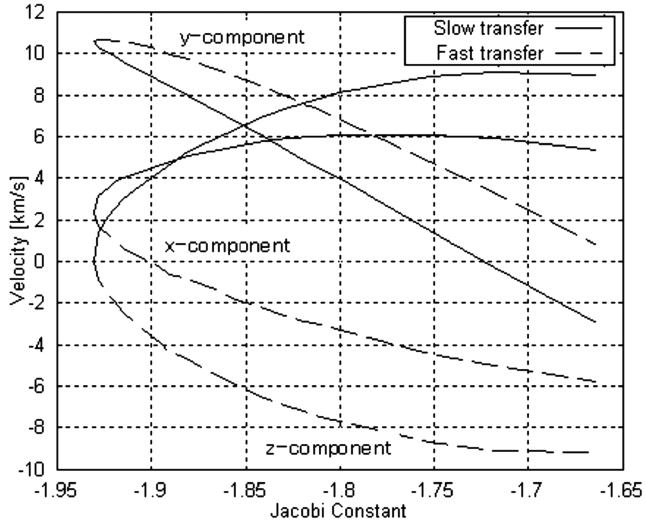

Fig. 5 Velocity of periapsis of Earth *L*1 unstable manifolds as a function of the Jacobi constant.

On the other hand, Figs. 6 and 7 show the position and the velocity of periapsis of the Mars $L2$ stable manifolds near the Mars surface (altitude = 200 km) as a function of the Jacobi constant in the sun–Mars fixed frame. Similar to the Earth unstable manifolds, we wish to select small Halo orbits since the z direction component of velocity increases as the value of the Jacobi constant increases, as shown in Fig. 7. Moreover, the y direction component of velocity is negative with the small Halo orbit.

IV. Analysis of Linking Interplanetary Transfer Trajectories with the Stable/Unstable Manifolds

In this section, we investigate the applicability of escape and capture trajectories to and from Halo orbits to interplanetary transfer missions, using impulsive maneuvers at the periapsis of the manifolds. We assume that the interplanetary transfer trajectories are approximated by a patched conic method. We concentrate our attention on finding a connection between the manifolds of the Earth Halo orbits on escape and the manifolds of Mars Halo orbits on capture, although these results can be applied to other planets of the solar system as well.

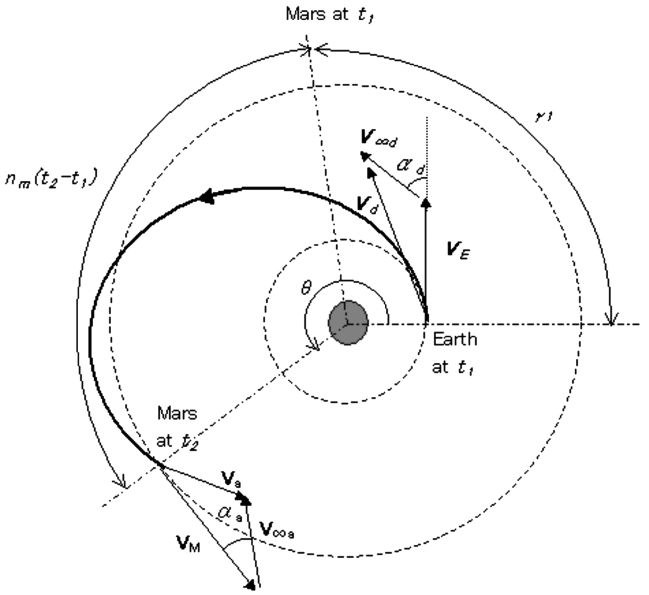

Fig. 8 Interplanetary transfer from Earth to Mars.

A. Interplanetary Transfer from Earth to Mars

Figure 8 shows a general elliptic trajectory of the Earth–Mars interplanetary transfer. The inner and outer circles correspond to Earth and Mars orbit, respectively. Symbols v_E and v_M are the Earth and Mars orbital velocities. At Earth departure a ΔV is added to the perigee speed to create a hyperbolic velocity $v_{\infty,d}$ to escape from the Earth. Subsequently, the spacecraft arrives at Mars with the arrival hyperbolic excess velocity $v_{\infty,a}$. A constraint for the interplanetary transfer is the required phase angle $\gamma 1$, which is the difference between the spacecraft transfer angle and an orbital motion of Mars during the transfer, as shown in Fig. 8. The orbital motion of Mars between the departure time at Earth t_1 and the arrival time at Mars t_2 is given by $n_m(t_2 - t_1)$, where n_m is the mean motion of Mars.

B. Connection Between Interplanetary Trajectories with Escape Trajectories

The location of perigee of departure hyperbolic trajectories from the Earth for interplanetary transfers is discussed in this section. These perigee points would be used to perform escape maneuvers for transfer to Mars.

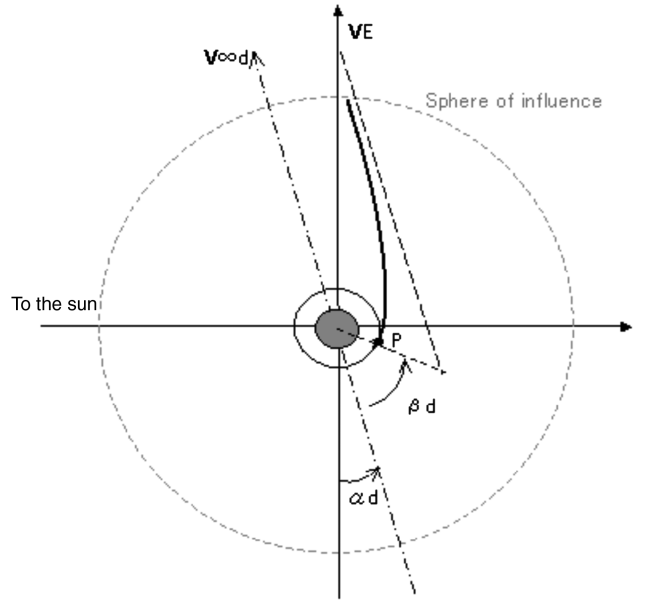

Fig. 9 Spacecraft departure trajectory for the interplanetary transfer from Earth to Mars.

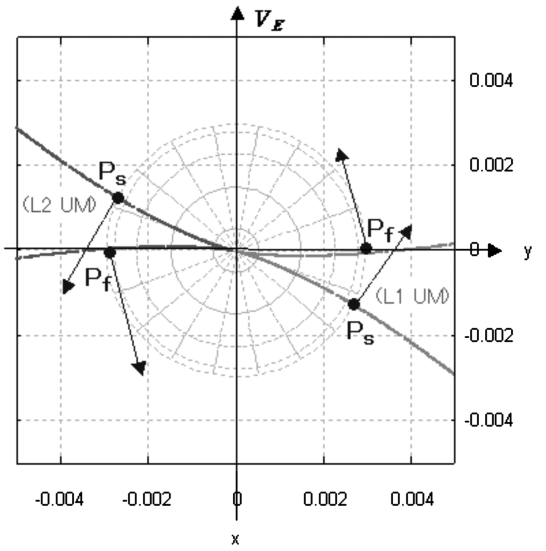

Fig. 10 Location of periapsis of the Earth $L1$ and $L2$ unstable manifolds in the ecliptic plane. The center circle represents the Earth.

Figure 9 shows periapsis of the departure hyperbola P in the ecliptic plane. The direction of the departure excess hyperbolic velocity relative to the orientation of the Earth orbital velocity vector is expressed by

$$\alpha_d = \cos^{-1}\left(\frac{\boldsymbol{v}_E \cdot \boldsymbol{v}_{\infty,d}}{|\boldsymbol{v}_E||\boldsymbol{v}_{\infty,d}|}\right) \tag{1}$$

The orientation of periapsis location relative to the direction of $v_{\infty,d}$ is represented by

$$\beta_d = \cos^{-1}\left(\frac{1}{1+\frac{(r_E+h)|\boldsymbol{v}_{\infty,d}|^2}{\mu_E}}\right) \tag{2}$$

where r_E and μ_E are the radius and the gravitational parameter of the Earth, respectively, and h is perigee altitude. The values of β_d depend on the magnitude of the departure hyperbolic excess velocity if the perigee altitude is fixed. The value of phase angles α_d and β_d become 0 and 29.2 deg, respectively, in the case of the Earth–Mars Hohmann transfer.

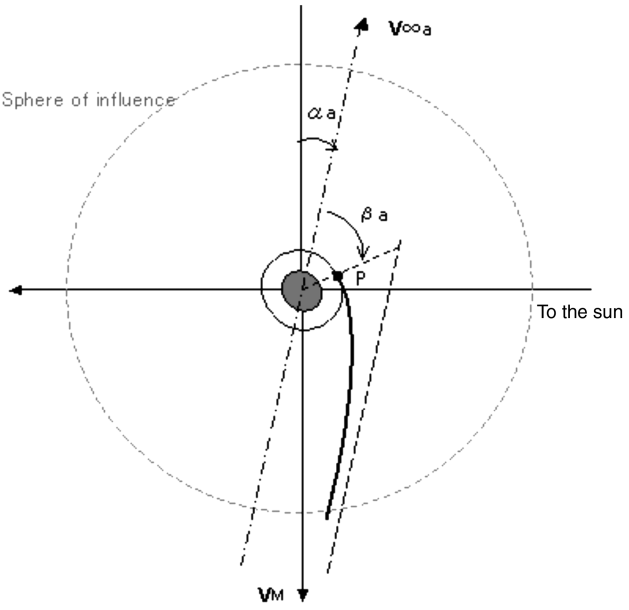

Fig. 11 Spacecraft approach trajectory for the interplanetary transfer from Earth to Mars.

Next, the location and velocity of the periapsis of Earth unstable manifolds are discussed. As mentioned before, the position and the velocity of the manifold periapsis depends on the value of the Jacobi constant. Figure 10 shows an example periapsis location of the Earth $L1$ and $L2$ unstable manifold (UM) for $J = -1.75$ at the altitude $h = 300$ km, and each arrow indicates the direction of velocity of the Earth unstable manifolds at the periapsis when the z component of velocity is small. Here, P_s is periapsis of the slow escape transfer and P_f is periapsis of the fast escape transfer. For a general spacecraft transfer from Earth to Mars, the departure hyperbolic express velocity $v_{\infty,d}$ is added to the direction of the Earth orbital velocity. Therefore, the Earth $L1$ unstable manifolds would be selected to connect with the interplanetary trajectory, rather than Earth $L2$ unstable manifolds.

C. Connection Between Interplanetary Trajectories with Capture Trajectories

Next, the periapsis locations of arrival hyperbolic trajectories after an interplanetary transfer are investigated. Figure 11 represents a schematic diagram of the approach trajectory to Mars after the interplanetary transfer. The periapsis point P at Mars is at an assumed altitude of $h = 200$ km in the ecliptic plane. A phase angle α_a gives the orientation of the hyperbolic arrival velocity $v_{\infty,a}$ with respect to the direction opposite to Mars's velocity, and β_a gives the orientation of the periapsis point ($h = 200$ km) with respect to $v_{\infty,a}$. These phase angles α_a and β_a are expressed as

$$\alpha_a = \cos^{-1}\left(\frac{\boldsymbol{v}_M \cdot \boldsymbol{v}_{\infty,a}}{|\boldsymbol{v}_M||\boldsymbol{v}_{\infty,a}|}\right) \tag{3}$$

$$\beta_a = \cos^{-1}\left(\frac{1}{1 + \frac{(r_M+h)|\boldsymbol{v}_{\infty,a}|^2}{\mu_M}}\right) \tag{4}$$

where r_M and μ_M are the radius of Mars and the gravitational parameter of Mars, respectively. For comparison, α_a is 0 and β_a is equal to 51.1 deg in the case of the Earth–Mars Hohmann transfer case.

Now, consider the location and velocity of the periapsis point of Mars's stable manifolds. Figure 12 shows an example periapsis location of the Mars $L1$ and $L2$ stable manifold (SM) for $J = -1.75$ at the altitude $h = 200$ km, where each arrow indicates the velocity direction of the stable manifolds at periapsis when the z component of velocity is small. Here, P_s is periapsis of the slow capture transfer and P_f is periapsis of the fast capture transfer. The direction of the capture hyperbolic velocity $v_{\infty,a}$ should be in the opposite direction of Mars's velocity in the case of transfers from Earth to Mars. Thus, the Mars $L2$ stable manifold is chosen to connect with the interplanetary trajectory instead of Mars $L1$ stable manifold.

D. Interplanetary Return from Mars to Earth

For a return mission, Fig. 13 shows a general interplanetary trajectory from Mars to Earth. The speed of the spacecraft must be reduced for it to go into a lower-energy transfer at Mars departure. Thus, the periapsis location of the departure hyperbolic trajectory from Mars to Earth is opposite to that of the transfer from Earth to Mars with respect to the origin (Fig. 14). Therefore, the Mars $L2$ unstable manifold is selected to connect with the interplanetary trajectory to the Earth. On the other hand, the periapsis of the arrival hyperbolic trajectory to Earth from Mars is located as in Fig. 15. Hence, the Earth $L1$ stable manifold is chosen to connect with the interplanetary trajectory from Mars.

For these reasons, putting spaceports at Earth $L1$ Halo orbit and Mars $L2$ Halo orbit is effective from a propellant standpoint.

E. Numerical Results in the Coplanar Circular Model Case

Now, a patched conic approximation for the interplanetary transfer is assumed linking the Earth and Mars manifolds associated with Halo orbits. We focus our attention on a transfer between Earth and Mars. However, these results can be applied to other planets of the

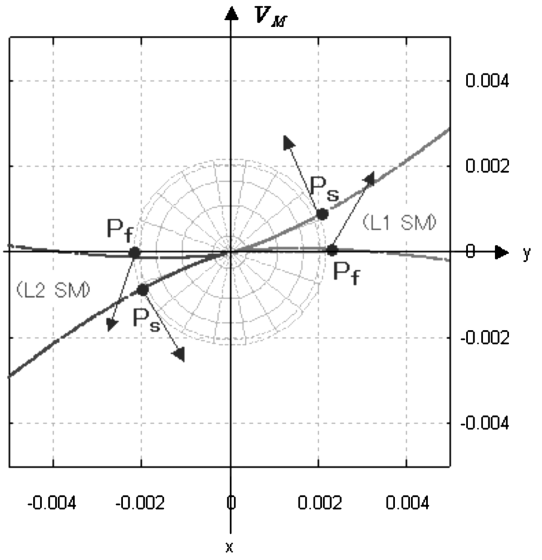

Fig. 12 Location of periapsis of the Mars $L1$ and $L2$ stable manifold in the ecliptic plane. The center circle represents Mars.

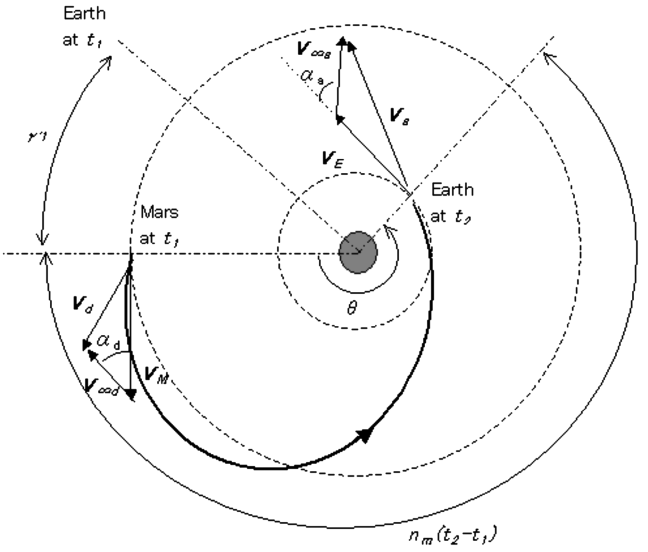

Fig. 13 Return interplanetary transfer from Mars to Earth.

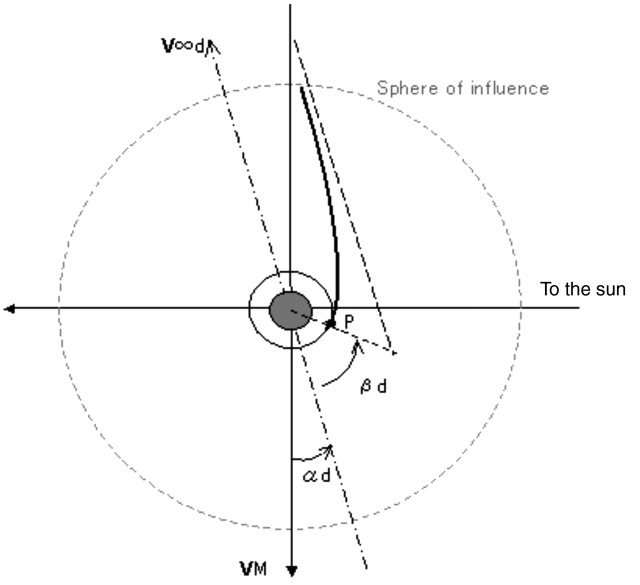

Fig. 14 Spacecraft departure trajectory for the interplanetary transfer from Mars to Earth.

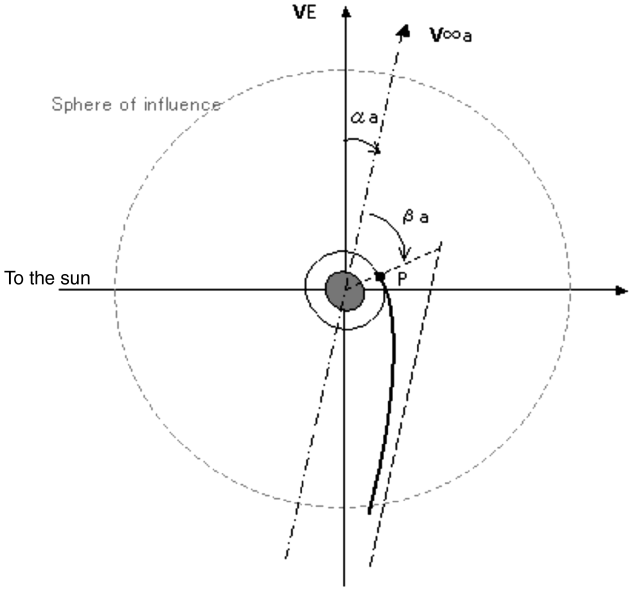

Fig. 15 Spacecraft arrival trajectory for the interplanetary transfer from Mars to Earth.

solar system as well. First, a transfer between an Earth $L1$ Halo orbit and a Mars $L2$ Halo orbit is discussed using the Hill three-body model around the Earth and Mars and using coplanar circular orbits between the Earth and Mars spheres of influence.

When we connect the Halo manifolds with interplanetary trajectories, assuming impulsive maneuvers near the surface of planets, the position of periapsis of the Halo manifolds should be matched with that of periapsis of the hyperbolic trajectories. Furthermore, it is more optimal when the velocity directions of the interplanetary trajectories and hyperbolic trajectories are aligned at periapsis. Therefore, we search the appropriate position and velocity direction of periapsis of hyperbolic trajectories for interplanetary transfer by varying the interplanetary transfer angle and the flight time between Earth and Mars step by step systematically, and search the appropriate position and velocity directions of periapsis of Halo manifolds by varying the size of the Halo orbit methodically. Here, the required cost for varying the size of the Halo orbits is small (about 40 m/s with nearly 120 days [16]), compared with the cost for an interplanetary transfer.

Tables 1 and 2 show the cost for a transfer from an Earth $L1$ Halo orbit to a Mars $L2$ Halo orbit. The columns called "$\Delta V_E\text{Phasing}_{\text{transfer}}$" and "$\Delta V_M\text{Phasing}_{\text{transfer}}$" represent the above-mentioned maneuvers to adjust the size of Earth and Mars Halo orbits for the Earth–Mars interplanetary transfer, respectively (Maneuver Nos. 4 and 9; see Table 9). "$\Delta V_E\text{Halo}_{\text{depart}}$" and "$\Delta V_M\text{Halo}_{\text{insert}}\ldots$" indicate impulsive maneuvers to reduce the TOF of the Earth Halo escape and Mars Halo capture between periapsis of manifolds and points on Halo orbit (Nos. 5 and 8). In general, the TOF is long for the escape and capture on the Halo orbit using the unstable and stable manifolds because the manifolds orbit around the $L1/L2$ point several times. By applying small impulsive maneuvers at the periapsis of the manifold and at a point on the Halo orbit, the TOF can be decreased considerably [17]. "ΔV_EEscape" is performed at perigee of the unstable manifold of the Earth $L1$ Halo orbit for the interplanetary transfer (No. 6). "ΔV_MCapture" is used at periapsis of the stable manifold for the capture to Mars $L2$ Halo orbit (No. 7). "A_yE" and "A_yM" indicate y amplitudes of the Earth and Mars Halo orbits, meaning the optimal Earth and Mars Halo sizes for ΔV. As a result, interplanetary trajectories between Earth Halo orbits and Mars Halo orbits with reasonable total ΔV and TOF were found. The required ΔV is less than half that of Alonso and Howell (5.28 km/s), and the TOF is about a quarter of Alonso and Howell (2919 days) [18]. This is because impulsive maneuvers for interplanetary transfers are assumed to be applied near the surface of planets in this study, as opposed to being performed in deep space for the Alonso and Howell study. The same goes for a return transfer from Mars $L2$ Halo orbit to Earth $L1$ Halo orbit (Tables 3 and 4).

Table 1 Required ΔV for the transfer from Earth $L1$ Halo to Mars $L2$ Halo

Type	ΔV_E Phasing transfer	ΔV_E Halo depart	ΔV_E Escape	ΔV_M Capture	ΔV_M Halo insert	ΔV_M Phasing transfer	Total ΔV
Coplanar circular	0.04	∼0.09	0.82	0.91	∼0.04	0.04	∼1.94
Alonso and Howell [18]	2.83 (Link Earth unstable manifold to arc)			2.45 (Link arc to Mars stable manifold)			5.28

[a](ΔV in km/s)

Table 2 Required TOF for the transfer from Earth $L1$ Halo to Mars $L2$ Halo

Type	TOF Phasing transfer	TOF E.Halo ∼ E.Peri	TOF E.Peri ∼ M.Peri	TOF M.Peri ∼ M.Halo	TOF Phasing transfer	Total TOF	A_yE	A_yM
Coplanar circular	120	69	308	117	120	734	0.755	0.552
Alonso and Howell [18]			2919			2919	-	-

[a](TOF in days)

Table 3 Required ΔV for the return transfer from Mars $L2$ Halo to Earth $L1$ Halo

Type	ΔV_E Phasing transfer	ΔV_E Halo insert	ΔV_E Capture	ΔV_M Escape	ΔV_M Halo depart	ΔV_M Phasing transfer	Total ΔV
Coplanar circular	0.04	∼0.09	0.82	0.91	∼0.04	0.04	∼1.94

[a](ΔV in km/s)

Table 4 Required TOF for the return transfer from Mars $L2$ Halo to Earth $L1$ Halo

Type	TOF Phasing transfer	TOF E.Halo ∼ E.Peri	TOF E.Peri ∼ M.Peri	TOF M.Peri ∼ M.Halo	TOF Phasing transfer	Total TOF	A_yE	A_yM
Coplanar circular	120	69	308	117	120	734	0.755	0.552

[a](TOF in days, A_y in million km)

Table 5 Required ΔV for the transfer from Earth $L1$ Halo to Mars $L2$ Halo

Departure and arrival date	ΔV_E Phasing transfer	ΔV_E Halo depart	ΔV_E Escape	ΔV_M Capture	ΔV_M Halo insert	ΔV_M Phasing transfer	Total ΔV
Sep. 2009 ∼ Oct. 2010	0.04	0.09	0.88	0.93	0.04	0.04	2.02
Oct. 2011 ∼ Oct. 2012	0.04	0.06	0.69	1.01	0.04	0.04	1.88
Nov. 2013 ∼ Oct. 2014	0.04	0.06	0.56	1.10	0.04	0.04	1.84

[a](ΔV in km/s)

Table 6 Required TOF for the transfer from Earth $L1$ Halo to Mars $L2$ Halo

Departure and arrival date	TOF Phasing transfer	TOF E.Halo ∼ E.Peri	TOF E.Peri ∼ M.Peri	TOF M.Peri ∼ M.Halo	TOF Phasing transfer	Total TOF	A_yE	A_yM
Sep. 2009 ∼ Oct. 2010	120	62	384	117	120	803	0.743	0.571
Oct. 2011 ∼ Oct. 2012	120	69	356	117	120	782	0.729	0.558
Nov. 2013 ∼ Oct. 2014	120	69	318	117	120	744	0.739	0.547

[a](TOF in days, A_y in million km)

Table 7 Required ΔV for the return transfer from Mars $L2$ Halo to Earth $L1$ Halo

Departure and arrival date	ΔV_E Phasing transfer	ΔV_E Halo insert	ΔV_E Capture	ΔV_M Escape	ΔV_M Halo depart	ΔV_M Phasing transfer	Total ΔV
July 2011 ∼ July 2012	0.04	0.09	0.93	0.87	0.04	0.04	2.01
Aug. 2013 ∼ Aug. 2014	0.04	0.09	0.84	1.11	0.04	0.04	2.16
Oct. 2015 ∼ Sep. 2016	0.04	0.09	0.76	1.37	0.04	0.04	2.34

[a](ΔV in km/s)

Table 8 Required TOF for the return transfer from Mars $L2$ Halo to Earth $L1$ Halo

Departure and arrival date	TOF Phasing transfer	TOF E.Halo ∼ E.Peri	TOF M.Peri ∼ E.Peri	TOF M.Peri ∼ M.Halo	TOF Phasing transfer	Total TOF	A_yE	A_yM
July 2011 ∼ July 2012	120	62	380	117	120	799	0.758	0.578
Aug. 2013 ∼ Aug. 2014	120	62	390	117	120	809	0.789	0.584
Oct. 2015 ∼ Sep. 2016	120	62	361	117	120	780	0.817	0.576

[a](TOF in days, A_y in million km)

F. Numerical Results in the Ephemeris Model Case

Next, we consider a transfer between an Earth $L1$ Halo orbit and a Mars $L2$ Halo orbit in the Hill three-body model around the Earth and Mars and in the real ephemeris model between the Earth and Mars spheres of influence. In a manner similar to the simple model case, we investigate a solution to connect the Earth and Mars Halo manifolds with interplanetary trajectories by varying the departure and arrival dates to and from Earth and Mars systematically, and by varying the size of the Earth and Mars Halo orbits methodically, assuming impulsive maneuvers near the surface of planets.

Tables 5–8 show the ΔV and the TOF for a transfer from an Earth $L1$ Halo orbit to a Mars $L2$ Halo orbit, and for the return transfer from a Mars $L2$ Halo orbit to an Earth $L1$ Halo orbit using ephemeris data for a time interval between 2009 and 2015. It was found that Earth $L1$ Halo and Mars $L2$ Halo orbits could be connected for a reasonable ΔV and TOF as in the previous coplanar circular model case; however, those values differ by about 10% since the Earth and Mars orbits are not circular.

V. Application to Earth–Mars Transportation System

A. Application to Earth–Mars Transportation System Using Spaceports at Halo Orbits

In this section we make an application of our results to an Earth–Mars transportation system, between low Earth orbits (LEO) and low Mars orbits (LMO), using spaceports at Earth and Mars Halo orbits as discussed above, and compared with a direct transfer system.

Tables 9 and 10 show the required ΔV and TOF for a transfer between LEO (altitude = 300 km) and LMO (altitude = 200 km) via the Earth and Mars Halo orbits and for a direct transfer case using ephemeris data from 2009 to 2016. "ΔV_{LEO}" and "ΔV_{LMO}" are maneuvers for a transfer from LEO to Earth Halo orbit and from Mars Halo orbit to LMO, respectively, (Maneuver Nos. 1 and 12). "$\Delta V_E\mathrm{Halo}_{\mathrm{insert}}$" and "$\Delta V_M\mathrm{Halo}_{\mathrm{insert}}$" are performed to reduce TOF between LEO/LMO and Earth/Mars Halo orbit (Nos. 2 and 11), and "$\Delta V_E\mathrm{Phasing}_{\mathrm{LEO}}$" and "$\Delta V_M\mathrm{Phasing}_{\mathrm{LMO}}$" indicate phasing maneuvers to adjust the size of the Earth and Mars Halo orbits for transfers between LEO/LMO and Earth/Mars Halo orbits (Nos. 3 and 10). It was found that the required total ΔV for a transfer from LEO to LMO via Earth and Mars Halo orbits is slightly greater than that of the direct transfer, and the TOF is longer. The same could be said for return transfers from the LMO to LEO via Mars and Earth Halo orbits as shown in Tables 11 and 12.

Considering the round-trip transfer between LEO and LMO, phasing maneuvers to adjust the size of Earth and Mars Halo orbits for return interplanetary transfers ("$\Delta V_E\mathrm{Phasing}_{\mathrm{transfer}}$" and "$\Delta V_M\mathrm{Phasing}_{\mathrm{transfer}}$") are as small as mentioned before [16]. On the other hand, phasing maneuver to adjust the phase of an LMO for return interplanetary transfers could be large. From these results, the system using Halo orbits has no advantage over the direct transfer with respect to ΔV and TOF. However, in the next section we show that the system using Halo orbits is preferred in terms of total mass.

B. Evaluation of the Earth–Mars Transportation System Using Halo Orbits

The Earth–Mars transportation system using spaceports at Earth and Mars Halo orbits is evaluated in terms of spacecraft mass for the round-trip transfer. Table 13 shows the required wet mass for the round-trip transfer that starts from LEO in 2013. Here, we assume the following:

Table 9 Required ΔV for the transfer from LEO to LMO

Maneuver No. (No. for direct)	1	2	3	4	5	6 (i)	7 (ii)	8	9	10	11	12	
Transfer type (departure date from LEO)	ΔV LEO	ΔV_E Halo insert	ΔV_E Phasing LEO	ΔV_E Phasing transfer	ΔV_E Halo depart	ΔV_E Escape	ΔV_M Capture	ΔV_M Halo insert	ΔV_M Phasing transfer	ΔV_M Phasing LMO	ΔV_M Halo depart	ΔV LMO	Total ΔV
Via Halo (in 2009)	3.15	0.06	0.04	0.04	0.09	0.88	0.93	0.04	0.04	0.04	0.04	1.42	6.79
Direct (in 2009)	-	-	-	($0 \sim 5.0$)	-	3.67	2.03	-	($0 \sim 2.0$)	-	-	-	5.70 $\sim$12.70
Via Halo (in 2011)	3.15	0.06	0.04	0.04	0.06	0.69	1.01	0.04	0.04	0.04	0.04	1.42	6.62
Direct (in 2011)	-	-	-	($0 \sim 5.0$)	-	3.63	2.16	-	($0 \sim 2.0$)	-	-	-	5.79 $\sim$12.79
Via Halo (in 2013)	3.15	0.06	0.04	0.04	0.06	0.56	1.10	0.04	0.04	0.04	0.04	1.42	6.59
Direct (in 2013)	-	-	-	($0 \sim 5.0$)	-	3.64	2.39	-	($0 \sim 2.0$)	-	-	-	6.03 $\sim$13.03

[a](ΔV in km/s)

Table 10 Required TOF for the transfer from LEO to LMO

Transfer type (departure date from LEO)	TOF LEO $\sim$ *E*.Halo	TOF *E*.Phasing LEO	TOF *E*.Phasing Transfer	TOF *E*.Halo $\sim$ *E*.Peri	TOF *E*.Peri $\sim$ *M*.Peri	TOF *M*.Peri $\sim$ *M*.Halo	TOF *M*.Phasing transfer	TOF *M*.Phasing LMO	TOF *M*.Halo $\sim$ LMO	Total TOF
Via Halo (in 2009)	69	120	120	62	384	117	120	120	117	1226
Direct (in 2009)	-	-	-	-	322	-	-	-	-	322
Via Halo (in 2011)	69	120	120	69	356	117	120	120	117	1208
Direct (in 2011)	-	-	-	-	307	-	-	-	-	307
Via Halo (in 2013)	69	120	120	69	318	117	120	120	117	1170
Direct (in 2013)	-	-	-	-	294	-	-	-	-	294

[a](TOF in days)

Table 11 Required ΔV for the return transfer from LMO to LEO

Maneuvers No. (No. for direct)	24	23	22	21	20	19 (iv)	18 (iii)	17	16	15	14	13	
Transfer type (departure date from LMO)	ΔV LEO	ΔV_E Halo depart	ΔV_E Phasing LEO	ΔV_E Phasing transfer	ΔV_E Halo insert	ΔV_E Capture	ΔV_M Escape	ΔV_M Halo depart	ΔV_M Phasing transfer	ΔV_M Phasing LMO	ΔV_M Halo insert	ΔV LMO	Total ΔV
Via Halo (in 2011)	3.15	0.06	0.04	0.04	0.09	0.93	0.87	0.04	0.04	0.04	0.04	1.42	6.76
Direct (in 2011)	-	-	-	$(0 \sim 5.0)$	-	3.64	2.07	-	$(0 \sim 2.0)$	-	-	-	5.71 ($\sim$12.71)
Via Halo (in 2013)	3.15	0.06	0.04	0.04	0.09	0.84	1.11	0.04	0.04	0.04	0.04	1.42	6.91
Direct (in 2013)	-	-	-	$(0 \sim 5.0)$	-	3.79	2.06	-	$(0 \sim 2.0)$	-	-	-	5.85($\sim$12.85)
Via Halo (in 2015)	3.15	0.06	0.04	0.04	0.09	0.76	1.37	0.04	0.04	0.04	0.04	1.42	7.09
Direct (in 2015)	-	-	-	$(0 \sim 5.0)$	-	3.98	2.06	-	$(0 \sim 2.0)$	-	-	-	6.04 ($\sim$13.04)

[a](ΔV in km/s)

Table 12 Required TOF for the return transfer from LMO to LEO

Transfer type (departure date from LMO)	TOF LEO $\sim$ *E*.Halo	TOF *E*.Phasing LEO	TOF *E*.Phasing transfer	TOF *E*.Halo $\sim$ *E*.Peri	TOF *E*.Peri $\sim$ *M*.Peri	TOF *M*.Peri $\sim$ *M*.Halo	TOF *M*.Phasing transfer	TOF *M*.Phasing LMO	TOF *M*.Halo $\sim$ LMO	Total TOF
Via Halo (in 2011)	69	120	120	62	380	117	120	120	117	1225
Direct (in 2011)	-	-	-	-	329	-	-	-	-	329
Via Halo (in 2013)	69	120	120	62	390	117	120	120	117	1235
Direct (in 2013)	-	-	-	-	350	-	-	-	-	350
Via Halo (in 2015)	69	120	120	62	361	117	120	120	117	1206
Direct (in 2015)	-	-	-	-	229	-	-	-	-	229

[a](TOF in days)

Table 13 Required mass for the round-trip transfer between LEO and LMO (departure date from LEO in 2013 and departure date from LMO in 2015)

Type		Via Earth and Mars Halo orbits to leave propellant for return transfer						Direct
Section		LEO ∼ *E*.Halo	*E*.Halo ∼ *M*.Halo	*M*.Halo ∼ LMO	LMO ∼ *M*.Halo	*M*.Halo ∼ *E*.Halo	*E*.Halo ∼ LEO	LEO ∼ LMO
Dry mass	ΔV [km/s]	3.25	1.84	1.50	1.50	2.34	3.25	12.07∼
	Propellant ratio	0.669	0.465	0.399	0.399	0.548	0.669	0.983∼
	Payload mass	1	1	1	1	1	1	1
	Structure and bus mass	4	4	4	4	4	4	4
	Carried propellant mass	42.3	14.9	3.3	0	0	0	0
		$(b+c+d+e+f)$	$(c+d+e)$	(d)				
	Consumed propellant mass	95.6 (a)	17.3 (b)	5.5 (c)	3.3 (d)	6.1 (e)	10.1 (f)	289.1∼
	Wet mass	142.9	37.2	13.8	8.3	11.1	15.1	294.1∼

1) Payload mass carried during the round-trip transfer is normalized to one.

2) The specific impulse of the impulsive spacecraft propulsion unit is 300 s.

3) Structure and bus mass is four times heavier than the payload mass.

4) The propellant for the return from an Earth Halo orbit to LEO is left at a spaceport on an Earth Halo orbit on the way to LMO.

5) The propellant for return from a Mars Halo orbit to an Earth Halo orbit is left at a spaceport on a Mars Halo orbit on the way to LMO.

From Table 13, compared with direct transfers between LEO and LMO, it is shown that the mass of the Earth–Mars transportation system S/C is reduced by one-half when starting from LEO using spaceports on Earth and Mars Halo orbits to leave propellant for the return transfer. The reason is simply because it is not necessary to carry the entire propellant load for return to LMO. First, the propellant for returning from Earth Halo orbit to LEO [the value is 10.1 (unitless)] is left at the spaceport on an Earth Halo orbit. Also, the propellant necessary for returning from the Mars Halo orbit to the Earth Halo orbit (6.1) is left at the spaceport on a Mars Halo orbit. Consequently, the propellant for the transfer from LMO to Mars Halo orbit (3.3) should only be carried to LMO. Therefore, it can be concluded that this round-trip transportation system using spaceports at the Earth and Mars Halo orbits is very effective. For comparison, Fig. 16 shows the wet mass (the dry mass and the required propellant mass) starting from LEO in the case where propellant is left at neither of the spaceports, the case of leaving propellant only at the Earth spaceport, the case of leaving propellant at both Earth and Mars spaceports, and the case of direct transfer. Numbers in the figure ($1 \sim 24$ and $i \sim iv$) correspond to the maneuver numbers in Tables 9 and 11. It is clear that leaving propellant at both the Earth and Mars spaceports is the best strategy. In practice, we also have to take into account the additional cost for the station keeping of the spaceports and rendezvous maneuvers.

C. Application to Interplanetary Transfers Other than Mars

For transfers to outbound targets such as Mars, the Earth spaceport needs to be located at Earth's $L1$ Halo orbit. However, for transfers to inbound targets such as Venus, the Earth spaceport needs to be located at Earth's $L2$ Halo orbits. Heteroclinic orbits such as those used in the Genesis mission ($\Delta V \cong 37$ m/s and TOF $\cong 0.3$ years)

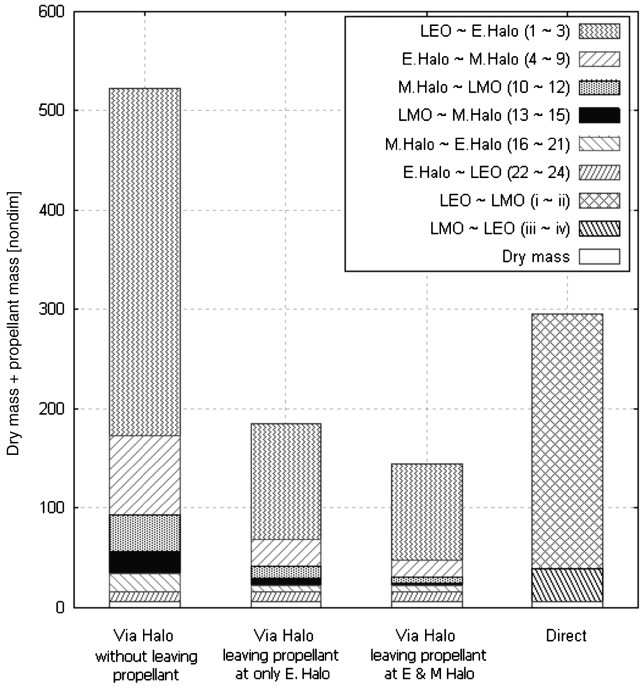

Fig. 16 Dry mass and propellant mass.

could be used to move the Earth spaceport between $L1$ Halo orbits and $L2$ Halo orbits [19–21].

VI. Conclusions

This paper discusses escape and capture trajectories to and from Halo orbits using impulsive maneuvers at periapsis of the manifold for interplanetary transfers, and provides a proposed application of these transfers to an Earth–Mars round-trip transportation system.

First, the characteristics of periapsis of Halo orbit manifolds near the surface of planets, where an impulsive maneuver would be performed for the interplanetary transfer, were investigated. Next, the links between an interplanetary trajectory and escape/capture trajectories to and from Halo orbits were analyzed. The survey found interplanetary trajectories between Earth $L1$ Halo orbits and Mars $L2$ Halo orbits with reasonable delta-V and flight time.

Finally, our strategy is applied to an Earth–Mars transportation system. The required delta-V for the round-trip transfer between the low Earth orbit and the low Mars orbit via spaceports on Earth and Mars Halo orbits becomes slightly larger than that of the direct round-trip transfer. However, an evaluation in terms of the required spacecraft wet mass for an Earth–Mars transportation system shows that by placing spaceports in Halo orbits, the wet mass starting from the low Earth orbit could be reduced by one-half compared with a direct transfer, by leaving propellant for return at spaceports at the Earth and Mars Halo orbits on the way to the low Mars orbit.

References

[1] Nakamiya, M., Scheeres, D., Yamakawa, H., and Yoshikawa, M., "Analysis of Capture Trajectories to Libration Points," *Journal of Guidance, Control, and Dynamics*, Vol. 31, No. 5, 2008, pp. 1344–1369. doi:10.2514/1.33796

[2] Farquhar, R. W., Dunham, D, W., Guo, Yan-ping, and McAdams, V. J., "Utilization of Libration Points for Human Exploration in the Sun–Earth–Moon System and Beyond," *Acta Astronautica*, Vol. 55, Nos. 3–9, 2004, pp. 687–700. doi:10.1016/j.actaastro.2004.05.021

[3] Marsden, J. E., and Ross, S. D."New Methods in Celestial Mechanics and Mission Design," *Bulletin of the American Mathematical Society*, Vol. 43, No. 1, 2006, pp. 43–73. doi:10.1090/S0273-0979-05-01085-2

[4] "JAXA Vision: JAXA 2005," http://www.jaxa.jp/2025/index_e.html.

[5] Matsumoto, M., and Kawaguchi, J., "Deep Space Quay and Solar Voyage Era," *The Sixth IAA International Conference on Low-Cost Planetary Missions*, International Academy of Astronautics, Paris, pp. 401–408.

[6] Nakamiya, M., and Yamakawa, H., "Earth Escape Trajectories Starting from $L2$ Point," *AIAA/AAS Astrodynamics Specialist Conference and Exhibit*, AIAA Paper No. 2006-6751, Keystone, CO, 21–24 Aug. 2006.

[7] Szebehely, V., *Theory of Orbits: The Restricted Problem of Three Bodies*, Academic Press, New York, 1967.

[8] Villac, B. F., and Scheeres, D. J., "Escaping Trajectories in the Hill Three-Body Problem and Applications," *Journal of Guidance, Control, and Dynamics*, Vol. 26, No. 2, 2003, pp. 224–232. doi:10.2514/2.5062

[9] Henon, M., "Numerical Exploration of the Restricted Problem 5. Hill's Case: Periodic Orbits and Their Stability," *Astronomy and Astrophysics*, Vol. 1, No. 2, 1969, pp. 223–238.

[10] Breakwell, J. V., and Brown, J. V., "The 'Halo' Family of 3-Dimensional Periodic Orbits in the Earth–Moon Restricted 3-Body Problem," *Celestial Mechanics*, Vol. 20, Nov. 1979, pp. 389–404. doi:10.1007/BF01230405

[11] Farquhar, R. W., "The Control and Use of Libration-Point Satellites," NASA TR R-346, 1970.

[12] Richardson, D. L., "Analytic Construction of Periodic Orbits About the Collinear Points," *Celestial Mechanics*, Vol. 22, Oct. 1980, pp. 241–253. doi:10.1007/BF01229511

[13] Howell, K. C., "Families of Orbits in the Vicinity of the Collinear Libration Points," *Journal of the Astronautical Sciences*, Vol. 49, No. 1, Jan.–March 2001, pp. 107–125.

[14] Simo, C., and Stuchi, T., "Central Stable/Unstable Manifolds and the Destruction of KAM Tori in the Planar Hill Problem," *Physica D*, Vol. 140, Nos. 1–2, 2000, pp. 1–32. doi:10.1016/S0167-2789(99)00211-0

[15] Gomez, G., Marcote, G., and Mondelo, J., "The Invariant Manifold Structure of the Spatial Hill's Problem," *Dynamical Systems: An International Journal*, Vol. 20, No. 1, 2005, pp. 115–147.

[16] Hiday, L. A., and Howell, K. C., "Impulsive Time-Free Transfers Between Halo Orbits," *AIAA/AAS Astrodynamics Conference*, AIAA Paper 92-4580, Hilton Head Island, SC, Aug. 1992.

[17] Nakamiya, M., Scheeres, D., Yamakawa, H., and Yoshikawa, M., "Preliminary Analysis of Space Transportation Systems with Spaceports Around Libration Points," *2008 AIAA/AAS Astrodynamics Specialist Conference*, AIAA Paper 2008-6625, Honolulu, HI, 18–21 Aug. 2008.

[18] Alonso, G., and Howell, K., "The Design of System-to-System Transfer Arcs Using Invariant Manifolds in the Multi-Body Problem," Ph.D., Dissertation, School of Aeronautics and Astronautics, Purdue Univ., West Lafayette, IN, Dec. 2006.

[19] Howell, K. C., Barden, B. T., and Lo, M. W., "Application of Dynamical Systems Theory to Trajectory Design for a Libration Point Mission," *Journal of the Astronautical Sciences*, Vol. 45, No. 2, April–June 1997, pp. 161–178.

[20] Canalias, E., and Masdemont, J. J., "Homoclinic and Heteroclinic Transfer Trajectories between Planar Lyapunov Orbits in the Sun–Earth and Earth–Moon Systems," *Discrete and Continuous Dynamical Systems A*, Vol. 14, No. 2, 2006, pp. 261–279.

[21] Arona, L., and Masdemont, J. J., "Computation of Heteroclinic Orbits Between Normally Hyperbolic Invariant 3-Spheres Foliated by 2-Dimensional Invariant Tori in Hill's Problem," *Discrete and Continuous Dynamical Systems*, Supplement 2007, pp. 64–74.